Morphological design of complex oxides during pulsed-laser deposition: The role of plasma-plume expansion

D. Del Gaudio [iD], C. T. Boone, K. Sallans, E. Mason, A. J. Williamson, S. Yarlagadda, Y. Turkulets [iD], J. T. Heron, I. Shalish [iD], and R. S. Goldman [iD]

View Online   Export Citation   CrossMark

Lock-in Amplifiers
... and more, from DC to 600 MHz   Watch

AIP Publishing

Morphological design of complex oxides during pulsed-laser deposition: The role of plasma-plume expansion

D. Del Gaudio,[1] [ID] C. T. Boone,[1,a)] K. Sallans,[1] E. Mason,[1] A. J. Williamson,[1] S. Yarlagadda,[1] Y. Turkulets,[2] [ID]
J. T. Heron,[1] I. Shalish,[2] [ID] and R. S. Goldman[1,b)] [ID]

AFFILIATIONS

[1]Materials Science and Engineering, University of Michigan, Ann Arbor, Michigan 48109, USA
[2]School of Electrical Engineering, Ben-Gurion University, Beer Sheva 84105, Israel

[a)]**Present address:** SELFA, California NanoSystems Institute at UCLA, Los Angeles, California, USA.
[b)]**Author to whom correspondence should be addressed:** rsgold@umich.edu

ABSTRACT

Complex oxides such as tin-doped indium oxide (ITO) are widely utilized as transparent conductors in a variety of functional devices. Typically, they are fabricated by sputtering, which often requires additional annealing to achieve high transparency and conductivity. Using pulsed laser deposition (PLD), both high transparency and high conductivity have been achieved without annealing, using instead selected gas species and pressures. However, the relative roles of Stranski-Krastanov-like and vapor-liquid-solid (VLS) growth modes during morphological transitions remain controversial. Here, we report on PLD of ITO in an inert-gas environment, identifying the role of plasma-plume expansion in the selection of VLS vs vapor-solid (VS) growth. For the lowest N_2 pressure, indium-tin droplet formation, followed by self-catalyzed VLS growth, is observed. With increasing N_2 pressure, a transition from VLS to VS growth is apparent. It is hypothesized that oxygen scattering at the lowest N_2 pressure induces a metal-rich plume, which leads to metal droplet formation, followed by VLS growth. As the N_2 pressure is increased, the plasma-plume and its metal-rich core are compressed, resulting in a transition to VS growth. This tunable compression of the plasma-plume offers a route to the morphological design of a wide range of functional complex oxide devices with tunable optical and electronic performance.

I. INTRODUCTION

Due to its high transparency and conductivity, tin-doped indium oxide (ITO) has been used as an electrode in solar cells, flat panel displays, Li-ion batteries, and light-emitting diodes (LEDs).[1] The high surface to volume ratios of ITO nanowire (NW) arrays are expected to lead to enhanced performance in numerous devices including solar cells,[2,3] gas sensors,[4,5] field emitters,[6] photodetectors,[7,8] photoelectrochemical cells,[9] and high-density memory devices.[10] ITO has recently been shown to possess strong nonlinear optical properties for near-infrared wavelengths, where its permittivity is vanishingly small (an epsilon-near-zero material).[11] ITO layers are typically prepared by sputtering, but this method requires postdeposition annealing to tailor transparency and conductivity, which depend strongly on crystallinity and morphology. Using pulsed laser deposition (PLD),

both high transparency and high conductivity can be achieved without annealing, thus extending the applicability of ITO to alternative substrates such as polymers and plastic. During PLD, control of the morphology to achieve vapor-liquid-solid (VLS) and vapor-solid (VS) growth has been reported,[12,13] typically via the selection of inert vs reactive gas species and/or tuning of the partial pressure. To date, the relative roles of Stranski-Krastanov-like and vapor-liquid-solid growth during this morphological transition remain controversial.

Here, we report on the PLD of ITO in an inert atmosphere, identifying the role of the plasma-plume expansion in the selection of VLS vs VS growth. For the lowest N_2 pressure, oxygen scattering yields a metal-rich plume leading to metal droplet formation, which facilitates VLS growth. As the N_2 pressure is increased, the lateral plasma-plume compression is identified as the mechanism

leading to a recovery of the oxygen-rich stoichiometry, resulting in a transition to VS growth. This approach to morphological design is applicable to a wide range of functional complex oxides.

II. METHODS

Pulsed laser deposition (PLD) was performed using a 248 nm KrF excimer laser with 20 ns pulse width. In preparation for PLD, sapphire substrates were sequentially sonicated in trichloroethylene, acetone, and isopropyl alcohol, followed by drying in N_2 gas. The substrates were subsequently attached to an Inconel platen using silver paint cured on a hot plate for 4 min at 90 °C. After cooling, the substrates were inserted into a load-lock and transferred into the PLD growth chamber with base pressure in the range of $5 \times 10^{-7} - 5 \times 10^{-6}$ Torr. During the pumping down of the load-lock, a target consisting of 90–10 wt. % In_2O_3-SnO_2 was preablated for 5 min. For PLD of ITO, we use an inert atmosphere (99.999% pure N_2) and 12,000 laser pulses with an energy of ~70 mJ and a spot size of ~0.09 cm^2, resulting in a fluence of ~0.8 J/cm^2. With a target-substrate separation of 7 cm, and a substrate temperature of 550 °C, similar to earlier studies,[12,13] several ITO layers were prepared using N_2 gas pressures, p_{N_2}, in the range of 7–740 mTorr, and pulse frequencies, f_{pulse}, in the range of 2.5–10 Hz. For these conditions, the plasma-plume spans approximately 1/3 to 1/2 of the target-substrate separation. Following deposition, power to the substrate heater was turned off, and the samples were allowed to cool in the N_2 inert atmosphere; in other words, the ITO target is the primary source of oxygen. We refer to those prepared at $p_{N_2} < 100$ mTorr and $p_{N_2} > 100$ mTorr as LoP and HiP, respectively. We also refer to those prepared with $f_{pulse} < 6$ Hz and $f_{pulse} > 6$ Hz as LoF and HiF, respectively. For each set of conditions, multiple samples were prepared. For most samples, the crystallinity and surface morphology were examined using θ-2θ x-ray diffraction (XRD) with Cu Kα$_1$ radiation, scanning electron microscopy (SEM) using an FEI XL30 SEM, and atomic force microscopy (AFM) using a Veeco Dimension Icon AFM.

III. RESULTS AND DISCUSSION

In Fig. 1, we present representative (a) x-ray diffraction spectra, corresponding SEM images of (b) LoF + LoP (2.5 Hz, 77 mTorr), (c) HiF + LoP (10 Hz, 7 mTorr), and (d) HiF + HiP (10 Hz, 740 mTorr) samples and AFM images of (f) HiF + HiP (10 Hz, 740 mTorr) samples, in comparison with (e) x-ray diffraction spectra from the ITO target and an ITO reference. For the ITO target [Fig. 1(e)], the observed reflections and their relative intensities are similar to those of the ITO reference[14] in Fig. 1(e). In both cases, the 2 2 2 reflection has the highest intensity, followed in order of decreasing intensity by 4 0 0 and 4 4 0, and 2 1 1 and 6 2 2.

For the deposited layers, the prominent reflection at 2θ = 41.675° corresponds to the 0 0 0 6 reflection of Al_2O_3, as expected for a c-plane sapphire substrate.[15] In addition, prominent reflections at 2θ = 17.50°, 30.56°, 35.43°, 39.78°, and 54.32°, corresponding to the 2 0 0, 2 2 2, 4 0 0, 4 2 0, and 6 0 0 reflections of the ITO reference in Fig. 1(e), respectively, indicate that crystalline ITO is present in all layers. Since the intensity of the 4 0 0 reflection is considerably higher than that of the 2 2 2 reflection, the layers are preferentially oriented
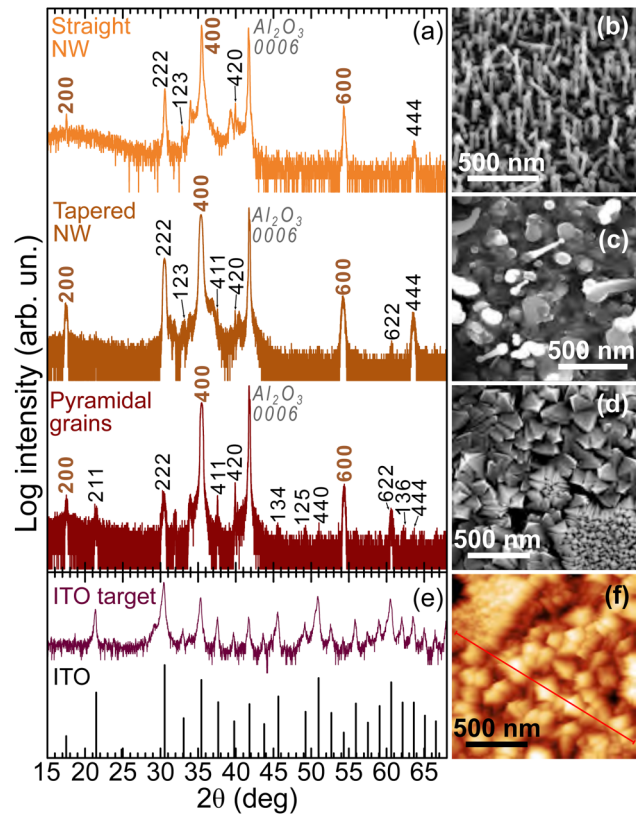

FIG. 1. (a) Plot of x-ray intensity vs 2θ for θ-2θ x-ray diffraction spectra from layers prepared using pulsed laser deposition (PLD) with low pressure/low pulse frequency (LoP + LoF—top), low pressure/high pulse frequency (LoP + HiF—middle), and high pressure/high pulse frequency (HiP + HiF—bottom), in comparison with spectra from (e) the In_2O_3-SnO_2 90–10 wt. % (ITO) ablation target and the ITO powder reference.[14] Corresponding scanning electron microscopy (SEM) images, revealing arrays of (b) straight smooth NWs, (c) tapered NWs, and (d) pyramidal grains, are shown on the right. An additional atomic force micrograph of pyramidal grains is shown in (f), with a line indicating the location of the line-cut shown in Fig. 3(i).

in the [1 0 0] direction normal to the surface of the substrate, consistent with earlier reports.[1,13]

We now consider the SEM images in Figs. 1(b)–1(d) and the AFM image in Fig. 1(f). In Fig. 1(b), arrays of upright nanowires (NWs) (length = 1.0 ± 0.1 μm; diameter = 40 ± 10 nm) with spherical tips, characteristic of VLS growth, are observed. In Fig. 1(c), arrays of tapered NWs (length = 700 ± 100 nm; diameter decreasing from 190 ± 10 nm to 80 ± 10 nm) with spherical tips, are observed. In some samples grown in LoF + LoP conditions, branching of the NW was observed, consistent with earlier reports.[1,12,13] The arrays of tapered NWs also contain a sparse concentration of nanoparticles (NPs), suggesting a contribution of VS growth in that case. Finally, in Figs. 1(d) and 1(f), arrays of pyramidal grains, 70–570 nm in diameter, due to VS growth, are apparent.

To quantify and compare the preferential orientations of the layers, we compute the texture coefficient $P(\boldsymbol{h}_i)$ for each detected

reflection $\boldsymbol{h}_i = h_i k_i l_i$:

$$P(\boldsymbol{h}_i) = \frac{I(\boldsymbol{h}_i)}{I_p(\boldsymbol{h}_i)} \left[\frac{1}{n} \sum_{i=1}^{n} \frac{I(\boldsymbol{h}_i)}{I_p(\boldsymbol{h}_i)} \right]^{-1}, \tag{1}$$

where $I(\boldsymbol{h}_i)$ and $I_p(\boldsymbol{h}_i)$ are the intensity of the measured and reference powder spectra for reflection $\boldsymbol{h}_i$ and n is the number of reflections considered in each spectrum. Thus, $P(\boldsymbol{h}_i) > 1$ indicates a preference for direction $[\boldsymbol{h}_i]$, while $P(\boldsymbol{h}_i) \leq 1$ indicates a lack of preference for direction $[\boldsymbol{h}_i]$. The texture coefficients computed for all observed reflections are shown in Table I. For all layers, the texture coefficients for 2 0 0, 4 0 0, and 6 0 0 reflections exceed 1, while those for all the others are less than 1, indicating a preferential [1 0 0] orientation.

To evaluate the [1 0 0]-orientation fraction, which is defined as the fraction of vertical [1 0 0]-oriented crystallites,[16] we compute the average $\frac{1}{n} \sum_{i=1}^{n} \eta(\boldsymbol{h}_i)$ for all the reflections $\boldsymbol{h}_i$ of

$$\eta(\boldsymbol{h}_i) = \sqrt{\frac{[1 - r(\boldsymbol{h}_i)]^3}{1 - r(\boldsymbol{h}_i)^3}}, \tag{2}$$

where $r(\boldsymbol{h}_i)$ is the parameter,[17]

$$r(\boldsymbol{h}_i) = \left[\frac{\sin^2 \alpha(\boldsymbol{h}_i)}{(\kappa(\boldsymbol{h}_i)/\kappa_p(\boldsymbol{h}_i))^{2/3} - \cos^2 \alpha(\boldsymbol{h}_i)} \right]^{\frac{1}{3}}, \tag{3}$$

with $\alpha(\boldsymbol{h}_i)$ being the angle between the direction $\boldsymbol{h}_i$ and the reference direction [4 0 0], $\kappa(\boldsymbol{h}_i) = I(4 0 0)/I(\boldsymbol{h}_i)$, and $\kappa_p(\boldsymbol{h}_i) = I_p(4 0 0)/I_p(\boldsymbol{h}_i)$. For the arrays of straight NWs, tapered NWs, and pyramidal grains, the [1 0 0]-orientation-fractions are 0.40 ± 0.15, 0.55 ± 0.17,

and 0.55 ± 0.18, respectively. The similarities in [1 0 0]-orientation-fractions across morphologies might indicate that orientation selection is determined by the [0 0 0 1]-oriented sapphire substrate. However, the lack of mutually aligned feature edges suggests the absence of ITO/sapphire epitaxy. Instead, the preferred [1 0 0] texture is likely determined by the minimization of interface energy, as supported by reports of preferred texture for NWs grown on Si or glass in Refs. 1, 12, and 13.

To explain the morphological evolution of the ITO layers, we consider the dynamics of the plasma-plume, as shown schematically in Fig. 2. For the LoP case, shown in Fig. 2(a), while the laser-ablated ITO plasma-plume expands, indium (115 amu), tin (119 amu), and oxygen (16 amu) are subject to collisions with the N_2 gas (28 amu).
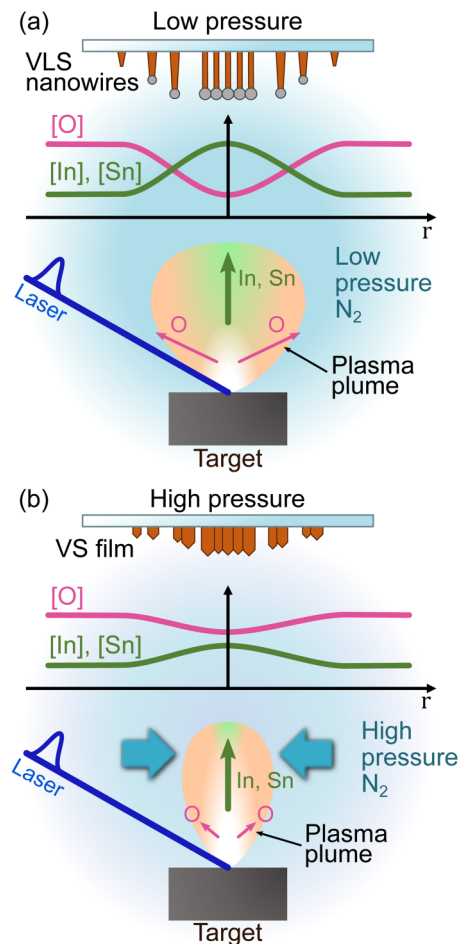

FIG. 2. Schematic of the plasma-plume expansion and its resulting stoichiometry. (a) For low N_2 pressure, oxygen is strongly scattered, resulting in a metal-rich core, as represented by the radial dependence of the oxygen, indium, and tin concentrations. The excess metal condenses in droplets on the substrate giving rise to VLS growth. (b) For higher N_2 pressure, the plasma-plume expansion is limited by the N_2, reducing the loss of oxygen, resulting in an oxygen-rich plasma, as indicated by the radial plot of oxygen, indium, and tin density. The oxygen-rich plasma is deposited on the substrate giving rise to VS growth.

TABLE I. Texture coefficients, $P(\boldsymbol{h}_i)$, for the arrays of straight NW, tapered NW, and pyramidal grains. When $P(\boldsymbol{h}_i) > 1$, $[\boldsymbol{h}_i]$ is a preferential orientation; when $P(\boldsymbol{h}_i) < 1$, $[\boldsymbol{h}_i]$ is not a preferential orientation. For clarity, the preferential orientations determined from this quantification, 6 0 0, 4 0 0, and 2 0 0, are shown in bold.

Reflection	Straight NW	Tapered NW	Pyramidal Grains
2 0 0	**1.86**	**2.95**	**2.58**
2 1 1	0.00	0.00	0.04
2 2 2	0.02	0.11	0.01
1 2 3	0.23	0.27	0.00
4 0 0	**1.99**	**3.63**	**2.42**
4 1 1	0.00	0.14	0.18
4 2 0	0.72	0.60	1.52
1 3 4	0.00	0.00	0.01
1 2 5	0.00	0.00	0.01
4 4 0	0.00	0.00	0.01
6 0 0	**2.16**	**3.13**	**3.21**
6 2 2	0.00	0.01	0.02
1 3 6	0.00	0.00	0.03
4 4 4	0.03	0.11	0.00

Due to the significant imbalance in masses between the metals (indium and tin) and the gases (oxygen and N_2), collisions with N_2 yield significant scattering of oxygen but negligible scattering of (the more massive) indium and tin, leading to the formation of a metal-rich plume core.[18,19] Once the plasma-plume reaches the substrate, the excess metal condenses into droplets that act as seeds for VLS NW growth.

For the HiP case shown in Fig. 2(b), on the other hand, oxygen dispersion due to collisions with N_2 is hindered by N_2 pressure-induced plume compression, resulting in a decrease in excess metal concentration at the plume core.[20] Interestingly, both lateral plume confinement and high-density fronts (shock-waves) have been previously observed within the plasma-plume. However, their potential connection to morphological design has not yet been realized.[21]

The morphology is also influenced by the diffusion of adsorbed metallic species (in this case, indium and tin) on the surface. To examine the effect of the plasma-plume expansion dynamics on the diffusion of adsorbed species, we consider the hydrodynamic model[22] of the evolution of the velocity v_{plume} of the plasma-plume

front in time t: $v_{plume} \propto p^{-1/5} t^{-3/5}$. Thus, with increasing pressure, p, the plasma-plume expansion is slowed. The slower plasma-plume expansion leads to lower kinetic energy for the atoms in the plasma, which induces lower diffusion rates. Thus, at low pressures, higher kinetic energy promotes condensation of metallic droplets, and, consequently, VLS growth. Conversely, at high pressures, the lower diffusion rate promotes crystallization of the ITO, rather than the formation of droplets, consistent with our observations.

Surface diffusion may also be enhanced by an increase in time between laser pulses (i.e., a reduced pulse frequency), or, vice-versa, surface diffusion may be reduced by an increased pulse frequency. For LoF, the adsorbed species enable droplet nucleation and coalescence, followed by VLS growth. Conversely, for the HiF case, the adsorbed species are unable to coalesce into droplets, while the higher oxygen supply rate favors metal-oxygen reaction and subsequent VS growth.[23]

The combined influences of the plasma-plume expansion and the subsequent diffusion of adsorbed species are illustrated in Fig. 3. For LoP + LoF, the metal-rich plasma-plume and low pulse
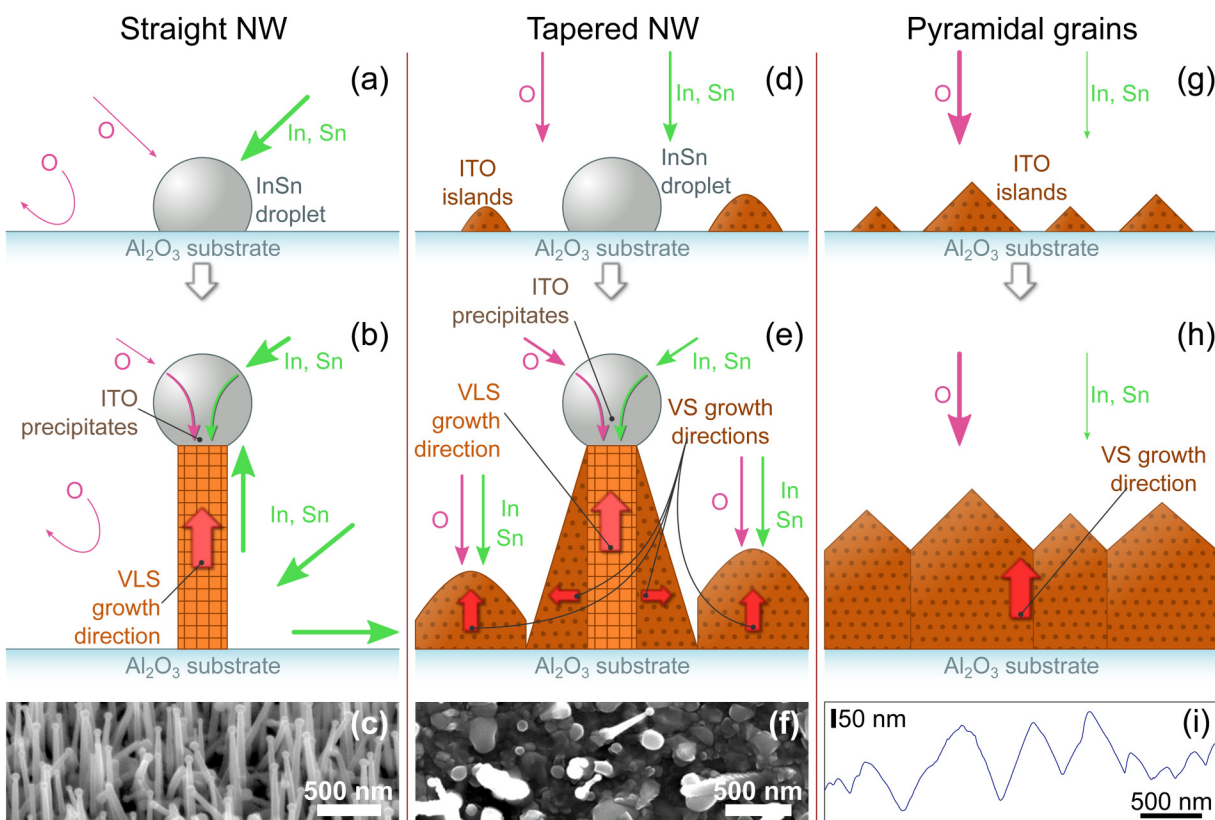

FIG. 3. Schematic of the growth mechanism for (a) straight smooth NW (VLS growth), (b) tapered NW (VLS + VS), and (c) polycrystalline film. Magenta arrows labeled "O" represent oxygen flux, while green arrows labeled "In, Sn" represent indium and tin flux. An increase (decrease) of thickness of these arrows represents an increase (decrease) in the intensity of the flux. (a) For the VLS growth mode, metal droplets are formed; then, (b) metal droplets act as catalysts for NW growth, resulting in (c) straight NW with spherical tips. (d) For concurrent VLS and VS growth modes, metal droplets and 3D islands nucleate; then, (e) metal droplets give rise to NW and VS growth gives rise to the polycrystal film among the NW, and overgrowth of film on the NW stems. The growth results in (h) tapered NW with spherical tips, surrounded by nanoparticles. (g) For the VS growth mode, only 3D islands form, giving rise to (h) polycrystalline columnar growth. (i) Line-cut from the AFM image of the VS ITO film in Fig. 1(f), showing the profile of the pyramidal grain tip.

frequency enable the formation of metal droplets, which act as catalysts as they become supersaturated with O, as shown in Fig. 3(a). The InSn alloy in the droplets reacts with the O, forming ITO, which precipitates at the nanodroplet/substrate interface, as shown in Fig. 3(b). With subsequent laser pulses, the ITO continues to be deposited at the base of the nanodroplets, inducing the formation of a column of high-quality ITO crystal, in the classic VLS growth mode. Indeed, as shown in Fig. 3(c), a dense array of high-aspect-ratio NWs, with spherical tips, consistent with the VLS growth mode, is apparent.

For the LoP + HiF case, the plasma-plume is metal-rich but the droplet nuclei are exposed to additional oxygen due to the frequent laser pulses. Consequently, in the early stages, as shown in Fig. 3(d), condensation of indium and tin leads to metal nanodroplet formation, while frequent laser pulses lead to local oxygen environments that promote the nucleation of 3D ITO islands. With subsequent laser pulses, the droplets give rise to VLS growth as in Fig. 3(c), and the 3D islands grow to form pyramidal grains in the VS growth mode. Additionally, the onset of VS growth causes additional lateral deposition of ITO on the NW walls, i.e., lower portions of the NW stem (base) are subject to the lateral ITO growth for longer time than later sections of the NW stem (top), leading to the formation of tapered NWs. In Fig. 3(f), the formation of tapered NW with spherical tips and pyramidal grains among the NW are apparent.

For the HiP + HiF case, due to the reduced lateral expansion of the plasma-plume, negligible excess metal is in contact with the sapphire substrate. The local oxygen-rich environment promotes the nucleation of 3D ITO islands, as shown in Fig. 3(g). With subsequent laser pulses, the VS growth of islands leads to the characteristic columnar growth that has been previously observed in several metal oxides,[24] as shown in Fig. 3(h). Indeed, in the line-cut from the AFM image in Fig. 1(f), shown in Fig. 3(i), pyramidal grains, consistent with pure VS growth, are apparent. Since the high-pressure-induced local oxygen-rich environment appears to govern the selection of VS vs VLS growth, similar results are expected for the HiP + LoF case.

IV. SUMMARY AND CONCLUSIONS

In summary, we have examined the morphological design of complex oxides during PLD in an inert atmosphere, identifying the role of the plasma-plume expansion on VLS vs VS growth. For the lowest pressure, oxygen scattering induces a metal-rich plasma core, leading to the coalescence of excess metal into droplets for VLS growth. As the pressure is increased, the plasma-plume and its metal core are laterally confined, leading instead to VS growth.

Thus, PLD is shown to afford a means to tune the growth mode of ITO between the direct VS and the liquid-metal-droplet-mediated VLS growth modes. Tuning the growth mode switches the resulting crystalline structure from a 3D polycrystalline film into an array of vertically aligned nanowires. Since the tuning directly corresponds to the compression/expansion of the plasma-plume, it can be directly controlled through the frequency and pressure parameters of the PLD growth. The same principle may be applicable to the PLD growth of other metal oxides for tailoring various material parameters such as transparency, conductivity, and dielectric constant. The tailoring of VLS vs VS growth via plasma-plume compression is also likely to be useful for designing nanostructures in a wide variety of complex metal-oxide systems.

REFERENCES

[1]C. O'Dwyer, M. Szachowicz, G. Visimberga, V. Lavayen, S. B. Newcomb, and C. M. S. Torres, Nat. Nanotechnol. **4**, 239 (2009).
[2]B. L. Williams, A. A. Taylor, B. G. Mendis, L. Phillips, L. Bowen, J. D. Major, and K. Durose, Appl. Phys. Lett. **104**, 053907 (2014).
[3]M. Yoshimura, E. Nakai, K. Tomioka, and T. Fukui, Appl. Phys. Lett. **103**, 243111 (2013).
[4]X. Y. Xue, Y. J. Chen, Y. G. Liu, S. L. Shi, Y. G. Wang, and T. H. Wang, Appl. Phys. Lett. **88**, 201907 (2006).
[5]R. Pruna, F. Palacio, M. López, J. Pérez, M. Mir, O. Blázquez, S. Hernández, and B. Garrido, Appl. Phys. Lett. **109**, 063109 (2016).
[6]Q. Wan, P. Feng, and T. H. Wang, Appl. Phys. Lett. **89**, 123102 (2006).
[7]S.-Q. Li, K. Sakoda, J. B. Ketterson, and R. P. H. Chang, Appl. Phys. Lett. **107**, 031104 (2015).
[8]D. S. Choi, M. Singh, H. Zhou, M. Milchak, and J. Hahm, Appl. Phys. Lett. **107**, 151110 (2015).
[9]J. Hong Noh, B. Ding, H. Soo Han, J. Seong Kim, J. Hoon Park, S. Baek Park, H. Suk Jung, J.-K. Lee, and K. Sun Hong, Appl. Phys. Lett. **100**, 084104 (2012).
[10]Q. Li, F. Yun, Y. Li, W. Ding, and Y. Zhang, Sci. Rep. **7**, 1600 (2017).
[11]M. Zahirul Alam, I. De Leon, and R. W. Boyd, Science **352**, 795 (2016).
[12]G. G. Khan, S. Ghosh, A. Sarkar, G. Mandal, G. D. Mukherjee, U. Manju, N. Banu, and B. N. Dev, J. Appl. Phys. **118**, 074303 (2015).
[13]E. Joanni, R. Savu, M. de Sousa Góes, P. R. Bueno, J. N. de Freitas, A. F. Nogueira, E. Longo, and J. A. Varela, Scr. Mater. **57**, 277 (2007).
[14]ICDD PDF Record No. 01-089-4597.
[15]ICDD PDF Record No. 00-046-1212.
[16]E. Zolotoyabko, J. Appl. Crystallogr. **42**, 513 (2009).
[17]W. A. Dollase, J. Appl. Crystallogr. **19**, 267 (1986).
[18]T. E. Itina, Nucl. Instrum. Methods Phys. Res. B **180**, 112 (2001).
[19]S. Canulescu, M. Döbeli, X. Yao, T. Lippert, S. Amoruso, and J. Schou, Phys. Rev. Mater. **1**, 073402 (2017).
[20]R. Eason, *Pulsed Laser Deposition* (Wiley-Interscience, 2006).
[21]B. N. Masina, S. Lafane, L. Wu, S. Abdelli-Messaci, T. Kerdja, and A. Forbes, Opt. Eng. **54**, 037106 (2015).
[22]P. L. G. Ventzek, R. M. Gilgenbach, C. H. Ching, and R. A. Lindley, J. Appl. Phys. **72**, 1696 (1992).
[23]J. M. Warrender and M. J. Aziz, Phys. Rev. B **76**, 045414 (2007).
[24]S. K. Choi and J. I. Lee, J. Vac. Sci. Technol. A **19**, 2043 (2001).